Pedestal radial flux measuring method to prevent impurity accumulation

Silvia Espinosa* and Peter J. Catto
MIT Plasma Science and Fusion Center, Cambridge, Massachusetts 02139, USA
(Dated: March 7, 2017)

Use of high-z wall materials attempts to shift the fusion challenge from heat handling to impurity removal. We demonstrate that not only the impurity density in-out asymmetry, but also the *poloidal* flow, have a major impact on the radial impurity flux direction. This realization provides the first method of measuring the flux from available diagnostics, without the need of a computationally demanding kinetic calculation of the full bulk ion response. Moreover, it affords insight into optimal tokamak operation to avoid impurity accumulation while allowing free fueling.

I. INTRODUCTION

Tokamaks are currently challenged by the large radiative energy losses produced when highly charged divertor impurities are absorbed through the pedestal and accumulate in the core of the plasma [1]. This can compromise tokamak performance in JET-ITL [2–4] and ASDEX-Upgrade [5], that mimic the ITER tungsten divertor, and in Alcator C-Mod with its molybdenum divertors [6].

Fusion performance can be substantially improved by reducing the inward radial impurity flux and, even better, changing its sign such that impurities are naturally pumped out of the plasma core. To preserve ambipolarity [7], background ions that fuel the plasma must go inward when the impurities go outward. Determining how to measure radial impurity flux across the pedestal and discovering its driving forces could thus be used to optimize tokamak operation to prevent impurity accumulation while providing natural fueling.

It has been suggested [8, 9] that the sudden transition between states of low (L) and high (H) confinement, the L-H transition, involves the reduction of turbulence by the strongly sheared radial electric field in the pedestal. For H-mode pedestals, the amplitudes of the turbulence may be only large enough to affect higher order phenomena in a poloidal gyroradius expansion, such as heat transport. Neoclassical collisional theory may then be expected to and is normally assumed [7, 10–14] to properly treat lower order phenomena, such as flows.

Specifically, an impure tokamak edge is often modeled [7] by allowing the flows to be large enough that the friction of the collisional highly-charged impurity species with the banana [7], Pfirsch-Schlüter [10] or plateau [11] main ions competes with the parallel impurity pressure gradient and parallel electric field. In contrast to [12–14], the flows are assumed smaller than the impurity thermal velocity in order to self-consistently neglect the inertial force.

The parallel friction is related to the flux-surface-averaged radial impurity flux [7], by employing conservation of toroidal momentum for the impurities. For the low flow ordering, the poloidal electric field rearranges the impurities poloidally on a pedestal flux surface to minimize the parallel friction with the background ions and thereby allow inboard impurity accumulation [7].

Impurity peaking on the inboard side is observed in tokamaks such as Alcator C-Mod [15–17], ASDEX-U [18, 19] and JET [20]. In addition, up-down asymmetries have also been detected on tokamaks such as Alcator A [21], PLT [22], PDX [23], ASDEX [24], Compass-C [25] and Alcator C-Mod [26–28].

Charge-exchange recombination spectroscopy [18, 29, 30] is used to measure the outboard (LFS) and inboard (HFS) boron density, temperature and importantly poloidal and toroidal mean flow radial profiles in the midplane pedestal region of Alcator C-Mod and ASDEX-U.

In general, a calculation of the impurity radial flux requires solving the main ion kinetic equation. Insightful solutions have been obtained at large aspect ratio for trace impurities or when impurity-ion collisions dominate over ion-ion collisions [12]. However, a numerical approach is needed in realistic situations with non-trace impurities having strong poloidal variation.

Here we illustrate how available diagnostics can be used to bypass the computationally demanding calculation of these kinetic effects by expressing them in terms of the poloidal flow. In Sec. II, we first show how the radial impurity flux in the pedestal can be re-expressed as a sum of two terms involving only the poloidal mean flow, the impurity density in-out asymmetry and the main ion radial density and temperature profiles. We then show how this form provides a precise means of calculating the neoclassical radial flux for non-trace impurities from diagnostics currently available, such as charge-exchange recombination spectroscopy and Thomson scattering. Although the methodology is illustrated for simplicity in the large aspect ratio limit, it can be expanded to realistic aspect ratios where its usage is of primary importance. In Sec. III, we discuss in detail the insight provided as to how best to optimize tokamak operation to prevent impurity accumulation and thereby provide natural fueling. Finally, the results are discussed and summarized in Sec. IV.

* sesp@mit.edu, espinosa@psfc.mit.edu

II. FIRST IMPURITY RADIAL FLOW DIAGNOSTIC

In this section, the main ion kinetic effects are related to the poloidal impurity flow. This allows us to express the neoclassical radial impurity flux as a function of measurements already available via charge-exchange recombination spectroscopy and Thomson scattering.

A. Sign convention

The axisymmetric tokamak magnetic field is given by $\mathbf{B} = I\boldsymbol{\nabla}\zeta + \boldsymbol{\nabla}\zeta \times \boldsymbol{\nabla}\psi$; where $I = RB_t$, with R the major radius and B_t the toroidal (subscript t) magnetic field. The poloidal (p) magnetic field is given by $RB_p = |\boldsymbol{\nabla}\psi|$, with $2\pi\psi$ the poloidal magnetic flux.

The direction of the poloidal and toroidal angles, denoted by θ and ζ respectively, is chosen such that $\mathbf{B}\cdot\boldsymbol{\nabla}\theta$ and the flux function I are positive. Moreover, the components of the mean flow $\mathbf{V}$ are considered positive when in the direction of the magnetic field. This sign convection is illustrated on an schematic tokamak cross-section in Fig. 1, and compared to that of Alcator C-Mod experiments [16] (Fig. 1a). While the sign convention adopted for the flows is the same as the C-Mod experimental one for normal or forward field operation (Fig. 1b), it is the opposite when the magnetic fields are reversed (Fig. 1c).

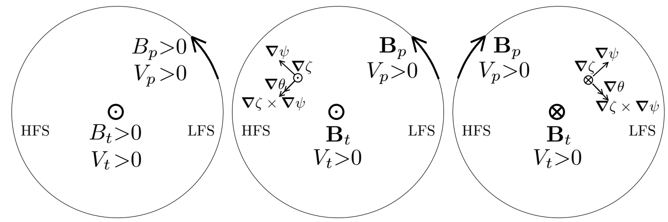

(a) C-Mod exp.[16] (b) Forward field (c) Reversed field

FIG. 1: Sign convention for C-Mod experiments (a), compared to ours for forward (b) and reversed (c) field.

B. Impurity-main ion friction

The plasma is taken to be composed of Maxwell-Boltzmann banana regime electrons and bulk ions (i) with charge number $z_i \sim 1$, together with a highly-charged collisional impurity (z) whose density n_z satisfies $z_z^2 n_z \lesssim z_i^2 n_i$. Although the impurity does not significantly alter the lowest-order quasineutrality, its density is large enough to affect the bulk ion dynamics by allowing main ion self-collisions and collisions with impurities to compete. Under these assumptions, the friction force exerted on the impurities by the bulk ions in the direction parallel ($\|$) to the magnetic field is [7]

$$F_{zi\|} = \frac{M_i \langle n_z\rangle}{B}\frac{\nu_{iz}}{n_z}\left[\frac{cI\langle p_i\rangle}{z_i e}\left(\frac{d\ln\langle p_i\rangle}{d\psi} - \frac{3}{2}\frac{d\ln T_i}{d\psi}\right)\left(\frac{B^2}{\langle B^2\rangle} - \frac{n_z}{\langle n_z\rangle}\right) + uB^2\left(\frac{n_z}{\langle n_z\rangle} - \left\langle\frac{B^2}{\langle B^2\rangle}\frac{n_z}{\langle n_z\rangle}\right\rangle\right)\right] \tag{1}$$

for arbitrary aspect ratio; where c and e are the speed of light and the magnitude of the electron charge. Each of the species has mass M and pressure $p = nT$, with T denoting the temperature.

The flux surface average of a quantity Q is defined as

$$\langle Q\rangle = \frac{\oint \frac{Qd\theta}{\mathbf{B}\cdot\boldsymbol{\nabla}\theta}}{\oint \frac{d\theta}{\mathbf{B}\cdot\boldsymbol{\nabla}\theta}} = \frac{\oint Qd\vartheta}{2\pi};$$

where ϑ is a modified poloidal angle coordinate, satisfying $\frac{d\vartheta}{\langle\mathbf{B}\cdot\boldsymbol{\nabla}\theta\rangle} = \frac{d\theta}{\mathbf{B}\cdot\boldsymbol{\nabla}\theta}$. The collision frequency of impurities with bulk ions divided by the impurity density,

$$\frac{\nu_{iz}}{n_z} = \frac{4\sqrt{2\pi}z_i^2 z_z^2 e^4 \ln\Lambda}{3M_i^{\frac{1}{2}}T_i^{\frac{3}{2}}}, \tag{2}$$

is a flux function; since the Coulomb logarithm $\ln\Lambda$ and the bulk ion temperature are taken to be flux functions. Moreover, the following integral over bulk ion velocity space $\mathbf{v}$,

$$u = \frac{3\sqrt{\pi}}{\sqrt{2}}\frac{T_i^{\frac{3}{2}}}{M_i^{\frac{3}{2}}}\int\frac{d^3v}{B}\frac{v_\|}{v^3}h_i, \tag{3}$$

is also a flux function for banana main ions [7]. Here the bulk ion kinetic response h_i is related to the gyroaveraged first-order main ion distribution function and vanishes in the trapped domain, but an explicit evaluation is not required. Indeed, one of the main purposes of this paper is to avoid the need to numerically solve the bulk ion kinetic equation to evaluate h_i.

C. Measuring the radial impurity flux

The radial component of the impurity particle flux, $\boldsymbol{\Gamma}_z = n_z\mathbf{V}_z$, is related to the parallel friction (1) by using the toroidal projection of the conservation of impurity parallel momentum equation [7]. Insight on a novel technique to measure the radial impurity flux is obtained by

Taylor expanding the flux surface averaged impurity radial flux for small inverse aspect ratio, $\epsilon \ll 1$, and using the solubility constraint, $\left\langle BF_{zi\|}\right\rangle = 0$, to find:

$$\begin{aligned}\frac{\left\langle \boldsymbol{\Gamma}_z \cdot \boldsymbol{\nabla}\psi \right\rangle}{\frac{cI}{z_z e \langle B^2 \rangle}} &= -\left\langle B^2 \right\rangle \left\langle \frac{F_{zi\|}}{B} \right\rangle = \left\langle \frac{-BF_{zi\|}}{1+(b^2-1)} \right\rangle \\ &= \left\langle BF_{zi\|}\left(b^2-1\right)\right\rangle \left[1+O\left(\epsilon\right)\right].\end{aligned} \tag{4}$$

Here both the poloidal variation of the square of the dimensionless magnetic field, $b^2 = \frac{B^2}{\langle B^2 \rangle}$, and the impurity density, $n = \frac{n_z}{\langle n_z \rangle}$, are retained.

Substituting the friction (1) into (4), noticing that $b^2 \left(n - \left\langle b^2 n \right\rangle\right) = (n-1)\left[1+O\left(\epsilon\right)\right]$, the radial impurity flux can be conveniently expressed in terms of flux functions to second-order accuracy as

$$\frac{\left\langle \boldsymbol{\Gamma}_z \cdot \boldsymbol{\nabla}\psi \right\rangle}{\frac{cI\langle \mathbf{B}\cdot\boldsymbol{\nabla}\theta\rangle\langle n_z\rangle\langle T_z\rangle}{z_z e \langle B^2 \rangle}} = \left\langle (n-1)\left(b^2-1\right)\right\rangle (g+U) - \left\langle \left(1-b^2\right)^2 \right\rangle g; \tag{5}$$

where, apart from the large aspect ratio expansion, only $n-1 \ll 1$ is required to neglect higher order corrections. Consequently, the impurity density is allowed in principle to have a stronger poloidal variation than the magnetic field, for instance, of order $\sqrt{\epsilon}$. The dimensionless coefficients

$$g = -\frac{cI}{z_i e}\frac{M_i\left\langle n_i\right\rangle}{\left\langle \mathbf{B}\cdot\boldsymbol{\nabla}\theta\right\rangle}\frac{\nu_{iz}}{n_z}\frac{T_i}{\left\langle T_z\right\rangle}\left(\frac{d\ln\left\langle p_i\right\rangle}{d\psi} - \frac{3}{2}\frac{d\ln T_i}{d\psi}\right) \tag{6}$$

and

$$U = \frac{u\left\langle B^2\right\rangle}{\left\langle T_z\right\rangle}\frac{M_i}{\left\langle \mathbf{B}\cdot\boldsymbol{\nabla}\theta\right\rangle}\frac{\nu_{iz}}{n_z} \tag{7}$$

indicate the contributions of the fluid and kinetic bulk ion responses, respectively. Here, $g \sim U \sim \frac{qR}{\lambda_z}\frac{\rho_{pi}}{L_i}$, with qR the connection length and λ_z the impurity mean free path taking into account both like and unlike collisions. The main ion poloidal Larmor radius and characteristic radial scale length are denoted by ρ_{pi} and L_i.

Charge-exchange recombination spectroscopy is used to measure the outboard (LFS) and inboard (HFS) impurity temperature, density, and poloidal and parallel mean flow radial profiles.

For illustrative purposes, a first-order cosinusoidal profile is considered for the known dimensionless magnetic field, $b^2 = 1 - 2\epsilon\cos\vartheta$; and a first-order Fourier profile for the dimensionless impurity density, with both a sinusoidal and a cosinusoidal term in order to allow for up-down and in-out asymmetries respectively. Only the measured impurity density in-out asymmetry term contributes to the following flux surface average needed to calculate the radial impurity flow (5),

$$\left\langle (n-1)\left(b^2-1\right)\right\rangle = \epsilon\frac{n_{HFS}-n_{LFS}}{n_{HFS}+n_{LFS}}, \tag{8}$$

which is positive for inboard impurity accumulation. For these profiles and trace impurities, it can be deduced from Sec. IV.A in [12] that there is inboard accumulation when g and $g+U$ have the same sign for low flows. As a consequence, the two terms of the radial impurity flux in (5) have opposite signs.

The same conclusion is drawn for very large gradients, i.e. friction dominating the parallel momentum equation. In this case, taking the large aspect ratio limit of Eq. (11) in [7] gives $\frac{n-1}{b^2-1} = \frac{g}{g+U}$. The results in this paper allow the impurity density poloidal variation to be larger than that of the magnetic field if $g+U \ll g$, although they are also valid when $g+U \sim g$.

Importantly, the impurity poloidal mean flow in [7], which can be measured by charge-exchange spectroscopy, can be used to obtain $g+U$ in (5) to lowest order by noticing that

$$\frac{n_z\mathbf{V}_z\cdot\boldsymbol{\nabla}\theta}{\mathbf{B}\cdot\boldsymbol{\nabla}\theta} = -\frac{cIT_i}{z_i e}\frac{\left\langle n_z\right\rangle}{\left\langle B^2\right\rangle}\left(\frac{d\ln\left\langle p_i\right\rangle}{d\psi} - \frac{3}{2}\frac{d\ln T_i}{d\psi}\right) + u\frac{\left\langle B^2 n_z\right\rangle}{\left\langle B^2\right\rangle\left\langle n_i\right\rangle} = \frac{\left\langle \mathbf{B}\cdot\boldsymbol{\nabla}\theta\right\rangle\left\langle n_z\right\rangle\left\langle T_z\right\rangle}{\frac{\nu_{iz}}{n_z}M_i\left\langle n_i\right\rangle\left\langle B^2\right\rangle}\left(g+U\right), \tag{9}$$

where we use $\left\langle b^2 n\right\rangle = 1 + O\left[\epsilon\left(n-1\right)\right]$. It can thus be observed that when $g+U$ is positive the poloidal impurity flow goes in the direction of the poloidal magnetic field.

Next, the radial gradient of the main ion density appearing in g in Eq. (6) can be obtained from Thomson scattering measurements of the radial pedestal electron density profile, by using lowest order quasineutrality, $z_i\left\langle n_i\right\rangle = \left\langle n_e\right\rangle$. The electron temperature is also available via Thomson scattering, while the impurity temperature is known from charge-exchange spectroscopy. Although all the temperatures are typically of the same order, it is better to use the impurity (rather than the electron) temperature to estimate the bulk ion temperature due to the more rapid ion-impurity energy equilibration. Note that g is negative if the descending slope of the logarithmic temperature is more than twice as steep as that of the logarithmic density for main ions, $\frac{d\ln T_i}{d\ln\langle n_i\rangle} > 2$, and positive otherwise.

III. SUGGESTED TOKAMAK OPERATION TO AVOID IMPURITY ACCUMULATION

The proposed method allows not only the measurement of the radial impurity flux but also provides insight into the favourable physical phenomena preventing impurity accumulation while achieving natural fueling. A detailed analysis of the profile characteristics that allow us identify optimal tokamak operation *'a posteriori'* is provided in this section, together with illustrative examples of its usage.

For completeness, suggestions on promising experimental procedures to favorably modify each term of the radial flux are discussed separately. Hopefully, these ideas will lead to further measurements on the effectiveness of these techniques on minimizing the inward radial impurity flux term while maximizing the outward one.

A. Impurity poloidal flow and density in-out asymmetry

The direction of the first component of the neoclassical pedestal radial impurity flux in (5) depends on both the impurity poloidal flow direction (9) and density in-out asymmetry (8). As explained in Table I, it removes impurities from the plasma core while absorbing fuel in the following two cases:

- The poloidal flow is in the direction of the magnetic field and there is HFS impurity accumulation.

- The poloidal flow and magnetic field are in opposite directions and there is LFS impurity accumulation.

Impurity poloidal flow in the direction of the magnetic field and HFS impurity accumulation have been observed in both ASDEX-U [19] and Alcator C-Mod [31] for different types of H-modes: EDA at lower (Fig. 4.4 in [31]) and higher safety factor (Fig. 4.5), ELM-free (Fig. 4.6) and ELMy (Fig. 4.7). These measurements, with $\mathbf{B}\times\nabla B$ towards the X-point, indicate a favorable outward neoclassical radial impurity flux for the first term.

Even though the physics included in the model has been limited here to illustrate how to infer radial fluxes from charge exchange and Thomson data, it is worth pointing out that there are practical methods of modifying tokamak in-out asymmetry such as neutral beam driven rotation or plasma heating. The centrifugal force associated with the toroidal rotation has been proven to push impurities outwards towards the LFS of each flux surface [12]. In contrast, neutral beam injection or ion cyclotron resonance heating (ICRH) of minority ions provide a mechanism for HFS impurity localization. Fast ions produced by neutral beam injection or ion cyclotron resonance heating of minority ions tend to concentrate on the outboard side. Quasi-neutrality then forces the highly charged impurities towards the HFS [14].

TABLE I: Direction of the first neoclassical pedestal radial impurity flux component in (5), as a function of the impurity poloidal flow direction and density in-out asymmetry obtainable by charge-exchange spectroscopy.

Direction of 1^{st} impurity radial flux term (5)		Impurity accumulation HFS	Impurity accumulation LFS
Poloidal impurity flow & magnetic field directions	Co $(g+U>0)$	Out	In
	Counter $(g+U<0)$	In	Out

TABLE II: Direction of the second neoclassical pedestal radial impurity flux component in (5), as a function of the ratio of main ion temperature to density gradients.

$\frac{d\ln T_i}{d\ln\langle n_i\rangle}$	g (6)	Direction of 2^{nd} impurity radial flux term (5)
<2	+	In
>2	-	Out

B. Main ion radial density and temperature profiles

The direction of the second neoclassical pedestal radial impurity flux component in (5) is determined by the radial profiles of the main ion temperature and density. As explained in Table II, it pumps out impurities when the background ion temperature is more than twice as steep as the density.

The appropriate tokamak operation can be identified by using a logarithmic plot of electron density gradient scale-length versus electron (or better yet, impurity, if available) temperature gradient scale-length. This is illustrated by Fig. 13 of [32], where only the 20% of plotted EDA and the 50% of ELM-free H-modes, with $\mathbf{B}\times\nabla\mathbf{B}$ towards and away from the X-point respectfully, are located in the region with $\eta = \frac{d\ln T_e}{d\ln n_e} > 2$. Those discharges exhibit favourable outward second term of the neoclassical radial impurity flux and are expected to prevent impurity accumulation while providing natural fueling.

There are several experimental techniques to affect the relative slope of the radial electron density and temperature profiles; such as fueling, mode excitation, recycling and impurity seeding. On the one hand, a high density region driven by gas puffing and heating power has been observed in the high field side scrape-of-layer at JET [33] and ASDEX-Upgrade [34]. In these cases the scrape-of-layer density is around ten times larger than at the separatrix and the dominant plasma fueling mechanism is diffusive neutral penetration. This effectively alters the electron pedestal profiles by shifting the density profile outwards [35]. The pedestal density height slightly increases while the height of the temperature significantly decreases, resulting on a lower pressure pedestal height (Fig. 3 in [36]).

On the other hand, impurity seeding can increase the relative pedestal pressure height by radiating input power away from the scrape-of-layer region, as observed at ASDEX-Upgrade [37] and JET [38, 39]. This method has been observed to significantly increase the steepness of the electron temperature while slightly reducing the steepness of the electron density (Fig. 3 in [37]) as desired. In addition, the electron density profile can be shifted inwards by exciting peeling-balloning modes in the pedestal as in DIII-D [40] or by reducing recycling by injecting Lithium as in NSTX [41, 42].

IV. SUMMARY

We provide the first practical way of evaluating the pedestal radial flux for non-trace impurities from measurements currently available. One of its main advantages is that it conveniently bypasses the computationally demanding kinetic calculation of the full bulk ion response by expressing the latter in terms of the poloidal impurity flow.

The neoclassical radial impurity flux has two components. The direction of the first is shown to be related to the impurity in-out asymmetry and the poloidal flow direction, both obtainable via change-exchange recombination spectroscopy. Inboard impurity accumulation with poloidal flow in the direction of the magnetic field or outboard impurity accumulation with opposite poloidal flow direction are desirable.

The direction of the second term depends on the relative slope of the main ion density and temperature profiles, which can be estimated by those of electrons and impurities and thus measured by Thomson scattering and charge-exchange spectroscopy respectively. A bulk ion temperature profile more than twice as steep as the density is shown to lead to impurity removal and fuel absorption by this term.

The novel measuring method can be used to optimize tokamak operation to reduce if not prevent impurity accumulation while providing natural fueling. For instance, the optimal H-mode type and parameters can be selected by identifying *'a posteriori'* the most beneficial physical behavior from a profile database.

In addition, our methodology may inspire the implementation of experimental techniques to actively and favorably modify the profiles, as well as make further measurements of their global effect on impurity confinement. For instance, toroidal rotation and ICRF minority heating can be used to push impurities outwards or inwards respectively. Moreover, mode excitation and scrape-of-layer high density reduction via impurity seeding can lead to a stronger and weaker radial variation of the electron temperature and density, respectively.

ACKNOWLEDGMENTS

We are indebted to S. C. Cowley for bringing the impurity accumulation problem to our attention. This research was supported by La Caixa Fellowship and DOE Grant DE-FG0291ER54109.

---

[1] T. C. Hender, P. Buratti, F. T. Casson, B. Alper, Y. F. Baranov, M. Baruzzo, C. D. Challis, F. Koechl, K. D. Lawson, C. Marchetto, M. F. F. Nave, T. Pütterich, S. Reyes Cortes, and JET Contributors, Nucl. Fusion **56**, 066002 (2016).
[2] G. F. Matthews, M. Beurskens, S. Brezinsek, M. Groth, E. Joffrin, A. Loving, M. Kear, M.-L. Mayoral, R. Neu, P. Prior, V. Riccardo, F. Rimini, M. Rubel, G. Sips, E. Villedieu, P. de Vries, M. L. Watkins, and EFDA-JET contributors, Phys. Scripta **2011**, 014001 (2011).
[3] R. Neu, G. Arnoux, M. Beurskens, V. Bobkov, S. Brezinsek, J. Bucalossi, G. Calabro, C. Challis, J. W. Coenen, E. de la Luna, P. C. de Vries, R. Dux, L. Frassinetti, C. Giroud, M. Groth, J. Hobirk, E. Joffrin, P. Lang, M. Lehnen, E. Lerche, T. Loarer, P. Lomas, G. Maddison, C. Maggi, G. Matthews, S. Marsen, M.-L. Mayoral, A. Meigs, P. Mertens, I. Nunes, V. Philipps, T. Pütterich, F. Rimini, M. Sertoli, B. Sieglin, A. C. C. Sips, D. van Eester, G. van Rooij, and JET-EFDA Contributors, Phys. Plasmas **20**, 056111 (2013).
[4] C. Angioni, P. Mantica, T. Pütterich, M. Valisa, M. Baruzzo, E. A. Belli, P. Belo, F. J. Casson, C. Challis, P. Drewelow, C. Giroud, N. Hawkes, T. C. Hender, J. Hobirk, T. Koskela, L. L. Taroni, C. F. Maggi, J. Mlynar, T. Odstrcil, M. L. Reinke, M. Romanelli, and JET EFDA contributors, Nucl. Fusion **54**, 083028 (2014).
[5] R. Neu, V. Bobkov, R. Dux, J. C. Fuchs, O. Gruber, A. Herrmann, A. Kallenbach, H. Maier, M. Mayer, T. Pütterich, V. Rohde, A. C. C. Sips, J. Stober, K. Sugiyama, and ASDEX Upgrade Team, Phys. Scripta **2009**, 014038 (2009).
[6] B. Lipschultz, D. Pappas, B. LaBombard, J. Rice, D. Smith, and S. Wukitch, Nucl. Fusion **41**, 585 (2001).
[7] P. Helander, Phys. Plasmas **5**, 3999 (1998).
[8] J. W. Connor and H. R. Wilson, Plasma Phys. Contr. F. **42**, R1 (2000).
[9] K. H. Burrell, Phys. Plasmas **4**, 1499 (1997).
[10] T. Fülöp and P. Helander, Phys. Plasmas **8**, 3305 (2001).

[11] M. Landreman, T. Fülöp, and D. Guszejnov, Phys. Plasmas **18**, 092507 (2011).
[12] T. Fülöp and P. Helander, Phys. Plasmas **6**, 3066 (1999).
[13] M. Romanelli and M. Ottaviani, Plasma Physics and Controlled Fusion **40**, 1767 (1998).
[14] C. Angioni and P. Helander, Plasma Physics and Controlled Fusion **56**, 124001 (2014).
[15] R. M. Churchill, B. Lipschultz, C. Theiler, and the Alcator C-Mod Team, Nucl. Fusion **53**, 122002 (2013).
[16] C. Theiler, R. M. Churchill, B. Lipschultz, M. Landreman, D. R. Ernst, J. W. Hughes, P. J. Catto, F. I. Parra, I. H. Hutchinson, M. L. Reinke, A. E. Hubbard, E. S. Marmar, J. T. Terry, J. R. Walk, and the Alcator C-Mod Team, Nucl. Fusion **54**, 083017 (2014).
[17] R. M. Churchill, C. Theiler, B. Lipschultz, I. H. Hutchinson, M. L. Reinke, D. Whyte, J. W. Hughes, P. Catto, M. Landreman, D. Ernst, C. S. Chang, R. Hager, A. Hubbard, P. Ennever, J. R. Walk, and A. C.-M. Team, Phys. Plasmas **22** (2015).
[18] T. Pütterich, E. Viezzer, R. Dux, R. M. McDermott, and the ASDEX Upgrade Team, Nucl. Fusion **52**, 083013 (2012).
[19] E. Viezzer, T. Pütterich, E. Fable, A. Bergmann, R. Dux, R. M. McDermott, R. M. Churchill, M. G. Dunne, and the ASDEX Upgrade Team, Plasma Phys. Contr. F. **55**, 124037 (2013).
[20] L. C. Ingesson, H. Chen, P. Helander, and M. J. Mantsinen, Plasma Phys. Contr. F. **42**, 161 (2000).
[21] J. L. Terry, E. S. Marmar, K. I. Chen, and H. W. Moos, Phys. Rev. Lett. **39**, 1615 (1977).
[22] K. H. Burrell and S. K. Wong, Nucl. Fusion **19**, 1571 (1979).
[23] K. Brau, S. Suckewer, and S. K. Wong, Nucl. Fusion **23**, 1657 (1983).
[24] P. Smeulders, Nucl. Fusion **26**, 267 (1986).
[25] R. D. Durst, Nucl. Fusion **32**, 2238 (1992).
[26] J. E. Rice, J. L. Terry, E. S. Marmar, and F. Bombarda, Nucl. Fusion **37**, 241 (1997).
[27] T. S. Pedersen, R. S. Granetz, E. S. Marmar, D. Mossessian, J. W. Hughes, I. H. Hutchinson, J. Terry, and J. E. Rice, Phys. Plasmas **9**, 4188 (2002).
[28] K. D. Marr, B. Lipschultz, P. J. Catto, R. M. McDermott, M. L. Reinke, and A. N. Simakov, Plasma Phys. Contr. F. **52**, 055010 (2010).
[29] R. M. McDermott, B. Lipschultz, J. W. Hughes, P. J. Catto, A. E. Hubbard, I. H. Hutchinson, R. S. Granetz, M. Greenwald, B. Labombard, K. Marr, M. L. Reinke, J. E. Rice, and D. Whyte, Phys. Plasmas **16**, 056103 (2009).
[30] R. M. Churchill, C. Theiler, B. Lipschultz, R. Dux, T. Pütterich, E. Viezzer, Alcator C-Mod Team, and ASDEX Upgrade Team, Rev. Sci. Instrum. **84**, 093505 (2013).
[31] R. M. Churchill, *Impurity Asymmetries in the Pedestal Region of the Alcator C-Mod Tokamak*, Ph.D. thesis, Massachusetts Institute of Technology (2014).
[32] D. G. Whyte, A. E. Hubbard, J. W. Hughes, B. Lipschultz, J. E. Rice, E. S. Marmar, M. Greenwald, I. Cziegler, A. Dominguez, T. Golfinopoulos, N. Howard, L. Lin, R. M. McDermott, M. Porkolab, M. L. Reinke, J. Terry, N. Tsujii, S. Wolfe, S. Wukitch, Y. Lin, and the Alcator C-Mod Team, Nucl. Fusion **50**, 105005 (2010).
[33] S. Potzel, M. Wischmeier, M. Bernert, R. Dux, F. Reimold, A. Scarabosio, S. Brezinsek, M. Clever, A. Huber, A. Meigs, and M. Stamp, J. Nucl. Mater. **463**, 541 (2015).
[34] S. Potzel, M. Wischmeier, M. Bernert, R. Dux, H. Müller, A. Scarabosio, and the ASDEX Upgrade Team, Nucl. Fusion **54**, 013001 (2014).
[35] M. Dunne, Nucl. Fusion **57**, 025002 (2017).
[36] M. G. Dunne, S. Potzel, F. Reimold, M. Wischmeier, E. Wolfrum, L. Frassinetti, M. Beurskens, P. Bilkova, M. Cavedon, R. Fischer, B. Kurzan, F. M. Laggner, R. M. McDermott, G. Tardini, E. Trier, E. Viezzer, M. Willensdorfer, T. E. M. Team, and T. A.-U. Team, Plasma Phys. Contr. F. **59**, 014017 (2017).
[37] J. Schweinzer, A. Sips, G. Tardini, P. Schneider, R. Fischer, J. Fuchs, O. Gruber, J. Hobirk, A. Kallenbach, R. McDermott, R. Neu, T. Pütterich, S. Rathgeber, J. Stober, J. Vicente, and the ASDEX Upgrade Team, Nucl. Fusion **51**, 113003 (2011).
[38] M. N. A. Beurskens, J. Schweinzer, C. Angioni, A. Burckhart, C. D. Challis, I. Chapman, R. Fischer, J. Flanagan, L. Frassinetti, C. Giroud, J. Hobirk, E. Joffrin, A. Kallenbach, M. Kempenaars, M. Leyland, P. Lomas, G. Maddison, M. Maslov, R. McDermott, R. Neu, I. Nunes, T. Osborne, F. Ryter, S. Saarelma, P. A. Schneider, P. Snyder, G. Tardini, E. Viezzer, E. Wolfrum, the ASDEX Upgrade Team, and J.-E. Contributors, Plasma Phys. Contr. F. **55**, 124043 (2013).
[39] C. Giroud, S. Jachmich, P. Jacquet, A. Järvinen, E. Lerche, F. Rimini, L. Aho-Mantila, N. Aiba, I. Balboa, P. Belo, C. Angioni, M. Beurskens, S. Brezinsek, F. J. Casson, I. Coffey, G. Cunningham, E. Delabie, S. Devaux, P. Drewelow, L. Frassinetti, A. Figueiredo, A. Huber, J. Hillesheim, L. Garzotti, M. Goniche, M. Groth, H.-T. Kim, M. Leyland, P. Lomas, G. Maddison, S. Marsen, G. Matthews, A. Meigs, S. Menmuir, T. Puetterich, G. van Rooij, S. Saarelma, M. Stamp, H. Urano, A. Webster, and J. E. Contributors, Plasma Physics and Controlled Fusion **57**, 035004 (2015).
[40] T. Osborne, G. Jackson, Z. Yan, R. Maingi, D. Mansfield, B. Grierson, C. Chrobak, A. McLean, S. Allen, D. Battaglia, A. Briesemeister, M. Fenstermacher, G. McKee, P. Snyder, and the DIII-D Team, Nucl. Fusion **55**, 063018 (2015).
[41] R. Maingi, S. M. Kaye, C. H. Skinner, D. P. Boyle, J. M. Canik, M. G. Bell, R. E. Bell, T. K. Gray, M. A. Jaworski, R. Kaita, H. W. Kugel, B. P. LeBlanc, D. K. Mansfield, T. H. Osborne, S. A. Sabbagh, and V. A. Soukhanovskii, Phys. Rev. Lett. **107**, 145004 (2011).
[42] M. G. Bell, H. W. Kugel, R. Kaita, L. E. Zakharov, H. Schneider, B. P. LeBlanc, D. Mansfield, R. E. Bell, R. Maingi, S. Ding, S. M. Kaye, S. F. Paul, S. P. Gerhardt, J. M. Canik, J. C. Hosea, G. Taylor, and the NSTX Research Team, Plasma Phys. Contr. F. **51**, 124054 (2009).